Engineering Analysis with Boundary Elements 81 (2017) 35–43

Contents lists available at ScienceDirect

Engineering Analysis with Boundary Elements

journal homepage: www.elsevier.com/locate/enganabound

# A continuous–discontinuous hybrid boundary node method for solving stress intensity factor

Fei Yan*, Xia-Ting Feng, Jia-He Lv, Shao-Jun Li

*State Key Laboratory of Geomechanics and Geotechnical Engineering, Institute of Rock and Soil Mechanics, Chinese Academy of Sciences, Wuhan 430071, China*

ARTICLE INFO

*Keywords:*
Meshless method
Dual reciprocity method
Hybrid boundary node method
Discontinuous shape function
Radial point interpolation method

ABSTRACT

A novel boundary type meshless method called continuous–discontinuous hybrid boundary node method is proposed in this paper, in which the enriched discontinuous shape function is developed to solve linear elastic crack problems. Firstly, the whole boundary is divided into several individual segments, and variables on each one of those segments are interpolated, respectively. For continuous segments, radial point interpolation method is employed. In regard to discontinuous segments, the enriched discontinuous basis functions combining with radial point interpolation method are developed for simulating the discontinuity of displacement and stress field on surfaces of crack, and the near tip asymptotic field functions are employed for simulating the high gradient of stress field around crack tip, so that high accuracy and discontinuity property of a crack can be easily described. Stress intensity factors are calculated directly using displacement extrapolation by displacement field near crack tip. Some numerical examples are shown that the present method is effective and can be widely applied in some practical engineering.



## 1. Introduction

For many structures, crack propagation is an important failure mechanism and requires accurate simulation essential for failure prediction. And stress intensity factors are important property, which are directly related to fracture propagation criteria. The analytical solutions of stress intensity factors are hardly got for many complex structures, so numerical methods must be applied for many cases.

Now many analytical and numerical methods are applied to solve fracture response and reliability of cracked structures. The most popular method recently is the finite element method (FEM). Although FEM is useful for many engineering analysis, even for fracture analysis of cracks, the method has serious limitations in some problems characterized by a continuous change in geometry of the domain under analysis. Crack propagation is a prime example in which a large number of remeshing is needed in the use of FEM. For FEM and some similar methods, the only viable option for dealing with moving cracks is remeshing during each discrete step, which is cumbersome and time-consuming. The boundary element method (BEM) [23] and dual boundary element method (DBEM) [24,25] which have certain advantages over FEM has been also applied to solve crack problems in past decades, but the same as FEM, element is inevitable in the calculation.

Meshfree or meshless methods have been developed rapidly in recent years. A class of meshfree and meshless methods appear to demonstrate significant special for the moving boundary problems typified by crack propagation. Such as smooth particle hydrodynamics (SPH) [11,15], diffuse element method (DEM) [19], element-free Galerkin method (EFGM) [4,12], meshless local Petrov–Galerkin method (MLPGM) [3], local boundary integral method [2], and meshless singular boundary method(MSBM) [8,9]. For those methods, the elements meshing is not used, since only a scattered set of nodal points is required in the domain of interest. Since no element connectivity is needed, the burdensome remeshing required by FEM is avoided.

Though all meshless methods do not need the element meshing for field variable interpolation, some of them require a background meshing for integration. For example, the EFG method [4,12] uses moving least square (MLS) for the shape function interpolation, and it does not require element mesh for variable interpolation. However, background element is inevitable for integration.

Appling MLS to the boundary integration equations, Mukherjee and Mukherjee proposed boundary node method (BNM) [16], which only requires to discretize the boundary. Although this method does not require an element mesh for the interpolation of the boundary variables, a background element is still necessary for integration. Based on BNM, Zhang et al. [39,40] proposed another boundary-type meshless method: hybrid boundary node method (HBNM). It abandons background elements and achieves a truly meshless method. Elements are required neither for interpolation nor for integration. However, it has a drawback of serious 'boundary layer effect'.

* Corresponding author.
*E-mail addresses:* fyan@whrsm.ac.cn, yanfei0324@163.com (F. Yan).

http://dx.doi.org/10.1016/j.enganabound.2017.05.002
Received 22 February 2017; Received in revised form 3 May 2017; Accepted 15 May 2017
0955-7997/

To avoid this shortcoming, Zhang and Yao further proposed the regular hybrid boundary node method [41,42], in which the source points of fundamental solution are located outside of the calculating domain. Although this method can avoid the singular integration and boundary layer effect, it creates some new problems. For example, how to arrange the positions of the source points? To overcome these problems, Wang et al. [30] presented a meshless singular hybrid node method for 2-D elasticity, and obtained satisfactory results by means of reasonable treatment of nearly singular integrals. And Miao et al. [13] proposed the rigid body motion approach to deal with singular integration and applied an adaptive integration scheme to solve boundary layer effect.

Those methods, however, can only be used for solving homogeneous problems. For inhomogeneous problems, domain integration is inevitable, and some methods are proposed for domain integral, for example, novel adaptive meshfree integration techniques are developed by Racz and Bui [26], besides, dual reciprocity method (DRM) was first proposed by Nardini and Brebbia [18] for elasto-dynamic problems in 1982 and extended by Wrobel and Brebbia [31] to time dependent diffusion in 1986. Based on HBNM, DRM is first introduced into HBNM, and a new truly meshless method dual hybrid boundary node method (DHBNM) is proposed by Yan et al. [36,38] which can be applied to inhomogeneous problems, dynamic problems and nonlinear problems and so on. Furthermore, based on radial point interpolation method and Taylor expansion, Yan et al. proposed a series of new hybrid boundary node methods [33,37], and by those methods some new shape function construction methods have been developed. Furthermore, combining radial point interpolation method, Yan et al. developed a new dual hybrid boundary node methods [34,35], later Yan et al. [32] developed a new shape function constructing method, named Shepard and Taylor interpolation method (STIM), by which no inversion operation is needed in the whole process of shape function constructing.

Unfortunately, the above methods based on a pure continuous theory are inadequate to describe such kinematic discontinuity of displacement field, and a discontinuity description in displacement field has been shown to be the necessity to describe the excessive discontinuous gap for two surfaces of a crack. Recently, a lot of continuous–discontinuous approaches have been proposed for solving those problems, for example, Simone et al. [28] and Oliver et al. [21] proposed a computational framework for the description of the continuous–discontinuous failure in a regularized strain-softening continuum; Oliver [20] employed strain softening constitutive equations to model strong discontinuities in solid mechanics; then Moes et al. [14] and Armero and Linder [1] and Stolarska et al. [29] developed the extended finite element method for analysis of crack growth, and so on.

DHBNM has some advantages, such as, dimensionality reduction, no element meshing, high accuracy and easily performance for large deformation, and it is widely used for inhomogeneous problems, nonlinear problems and dynamic problems, but its continuous property causes the difficult of application for crack propagation. Based on the boundary type meshless advantage property of hybrid boundary node method, a new continuous–discontinuous hybrid boundary node method is proposed to solve strong discontinuities problems in this paper. Firstly, the whole boundary is divided into several individual segments, and variables on each one of those segments are interpolated individually. For continuous segments, radial point interpolation method is employed. In regard to discontinuous segments, the enriched discontinuous basis functions combining with radial point interpolation method are developed for simulating the discontinuity of displacement and stress field on surfaces of fracture, and the near tip asymptotic field function is employed for simulating the singularity of crack tip stress field around the crack tip. Based on the above theory, a discontinuous hybrid boundary node method is proposed in this paper. And high accuracy and discontinuity property of a crack can be easily described in present method. This method keeps the 'boundary-only' and truly meshless method character of HBNM. The present work uses directly displacement extrapolation to calculate stress intensity factors. Besides, in order to simulate the singularity of stress field on the tip of fracture, and the enriched basis functions combined with radial point interpolation method are used near the tip of crack. Some numerical examples are shown that the present method is effective and can be widely applied in some practical engineering.

The discussions of this method arrange as following: the hybrid boundary node method will be discussed in Section 2. The enriched discontinuous interpolation is developed in Section 3. Some numerical implementation is demonstration in Section 4. The numerical examples for 2-D linear elastic crack problems are showed in Section 5. Finally, the paper will end with conclusions in Section 6.

## 2. Hybrid boundary node method

In this section, HBNM is introduced. Consider a 2D elasticity problem in domain $\Omega$ bounded by $\Gamma$. The basic equations are

$$\sigma_{ij,j} = b_i \tag{1}$$

$$\sigma_{ij} = 2G\varepsilon_{ij} + \lambda\varepsilon_{kk}\delta_{ij} \tag{2}$$

$$\varepsilon_{ij} = \frac{1}{2}\left(u_{i,j} + u_{j,i}\right) \tag{3}$$

where $b_i$ is the body force, $\lambda$ is the Lame constant and $G$ is the shear modulus.

The boundary conditions can be given as

$$u_i = \hat{u}_i \quad \text{on } \Gamma_u \tag{4}$$

$$\sigma_{ij}n_j = \hat{t}_i \quad \text{or } \Gamma_t \tag{5}$$

where $\hat{u}_i$ and $\hat{t}_i$ denote boundary node values and $n$ is the unit outward normal to the domain boundary $\Gamma$.

Solving the above equations, the second-order partial differential equations for the displacement components can be obtained as [37]

$$Gu_{i,kk} + \frac{G}{1-2\nu}u_{k,ki} = b_i \tag{6}$$

Applying DRM, the solution variables $u_i$ can be divided into two parts, i.e., the complementary solutions $u_i^c$ and the particular solutions $u_i^p$, that is

$$u_i = u_i^c + u_i^p \tag{7}$$

The particular solution $u_i^p$ has to satisfy the inhomogeneous equation as

$$Gu_{i,kk}^p + \frac{G}{1-2\nu}u_{k,ki}^p = b_i \tag{8}$$

On the other hand, the complementary solution $u_i^c$ must satisfy the homogeneous equation and the modified boundary conditions. It can be written in the form [37]

$$Gu_{i,kk}^c + \frac{G}{1-2\nu}u_{k,ki}^c = 0 \tag{9}$$

$$u_i^c = \hat{u}_i^c = \hat{u}_i - u_i^p \tag{10}$$

$$t_i^c = \hat{t}_i^c = \hat{t}_i - t_i^p \tag{11}$$

where $\hat{u}_i^c$, $\hat{t}_i^c$ denote complementary solutions on boundary node $i$.

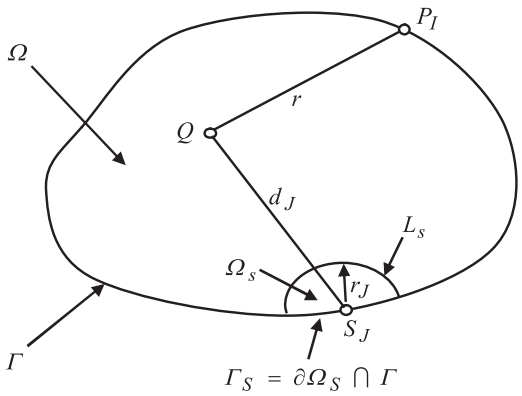


**Fig. 1.** Local domain and source point corresponding to $s_J$.

### 2.1. Variational principle

The total potential energy can be given as [16,39]

$$\Pi = \int_\Omega \frac{1}{2} u_{i,j} c_{ijkl} u_{kl} d\Omega - \int_\Omega \mathbf{u}^T \mathbf{b} d\Omega - \int_{\Gamma_t} \mathbf{u}^T \hat{\mathbf{t}} d\Gamma \tag{12}$$

where $\mathbf{u}$ is the displacement vector, $\hat{\mathbf{t}}$ is the boundary traction vector, and the coefficients $c_{ijkl} = \frac{2G\nu}{1-2\nu}\delta_{ij}\delta_{kl} + G\delta_{il}\delta_{jk}$.

There are three independent variables in the variational principle, namely the displacement in the domain, the displacement along the boundary and the force acting normal to boundary. They can be written as $\mathbf{u}$, $\tilde{\mathbf{u}}$ and $\tilde{\mathbf{t}}$, respectively. Boundary compatibility conditions $\tilde{\mathbf{u}} = \mathbf{u}$ and a set of Lagrange multipliers boundary tractions are introduced into Eq. (12).

Based on hybrid displacement variational principle, test function $h_J(Q)$ is used to replace the variational part, one can get [16,39]

$$\int_{\Gamma_S + L_S} (t_i - \tilde{t}_i) h_J(Q) d\Gamma - \int_{\Omega_S} \sigma_{ij,j} h_J(Q) d\Omega = 0 \tag{13}$$

$$\int_{\Gamma_S + L_S} (u_i - \tilde{u}_i) h_J(Q) d\Gamma = 0 \tag{14}$$

The shape and dimension of the sub-domains may be arbitrary. Obviously, a circle is the simplest regularly shaped sub-domain in the 2D space. The sub-domain $\Omega_s$ is chosen as the intersection of the domain $\Omega$ and a circle centered at a boundary node, $s_J$ (Fig. 1) [36,38], and the radius of the circle is $r_J$.

In Eqs. (13) and (14), the variable of $\tilde{u}_i$ and $\tilde{t}_i$ on $L_s$ are not defined. If $h_J(Q)$ can be selected in such a way that the integral over $L_s$ vanish, the problem can be solved successfully. Thus test function $h_J(Q)$ can be written in the form [16,39]

$$h_J(Q) = \begin{cases} \dfrac{\exp[-(d_J/c_J)^2] - \exp[-(r_J/c_J)^2]}{1 - \exp[-(r_J/c_J)^2]} & 0 \le d_J < r_J \\ 0 & d_J \ge r_J \end{cases} \tag{15}$$

where $d_J$ is the distance between the integral point, Q, in the domain and the nodal point, $s_J$. $c_J$ is a constant controlling the test function shape, $r_J$ is the radius of the sub-domain. On $L_S$, $d_J = r_J$, from Eq. (15), it can be seen that $h_J(Q)$ vanishes on the boundary.

Eqs. (13) and (14) can be rewritten as follows [16,39]

$$\int_{\Gamma_S} (t_i - \tilde{t}_i) h_J(Q) d\Gamma - \int_{\Omega_S} \sigma_{ij,j} h_J(Q) d\Omega = 0 \tag{16}$$

$$\int_{\Gamma_S} (u_i - \tilde{u}_i) h_J(Q) d\Gamma = 0 \tag{17}$$

### 2.2. The domain variables interpolation

The domain variables $\mathbf{u}$ and $\mathbf{t}$ are interpolated by the fundamental solution and can be written as

$$\mathbf{u} = \begin{Bmatrix} u_1 \\ u_2 \end{Bmatrix} = \sum_{I=1}^{N_t} \begin{bmatrix} u_{11}^I & u_{12}^I \\ u_{21}^I & u_{22}^I \end{bmatrix} \begin{Bmatrix} x_1^I \\ x_2^I \end{Bmatrix} \tag{18}$$

$$\mathbf{t} = \begin{Bmatrix} t_1 \\ t_2 \end{Bmatrix} = \sum_{I=1}^{N_t} \begin{bmatrix} t_{11}^I & t_{12}^I \\ t_{21}^I & t_{22}^I \end{bmatrix} \begin{Bmatrix} x_1^I \\ x_2^I \end{Bmatrix} \tag{19}$$

where $x_i^I$ is the unknown parameter, $N_t$ is the total boundary node number, $u_{ij}^I$ and $t_{ij}^I$ are the fundamental solution with the source point of $P^I$ (Fig. 1).

The fundamental solution of the 2-D plane strain elasticity problem is given by

$$u_{ij}^I = \frac{-1}{8\pi(1-\nu)G}\left[(3-4\nu)\delta_{ij}\ln(r) - r_{,i}r_{,j}\right] \tag{20}$$

$$t_{ij}^I = \frac{-1}{4\pi(1-\nu)r}\left\{\left[(1-2\nu)\delta_{ij} + 2r_{,i}r_{,j}\right]\frac{\partial r}{\partial n} + (1-2\nu)\left(r_{,i}n_j - r_{,j}n_i\right)\right\} \tag{21}$$

where $\delta$ is the Kronecker delta function, $r$ is the distance between the source point and the field point, $n_i$ is the outward normal to the boundary, $r_{,i}$ denotes $\frac{\partial r}{\partial x_i}$.

### 2.3. Hybrid boundary node method

From the above description, it is obvious that the second term of Eq. (16) only attributes to the principal diagonal of the matrix. Substituting discontinuous shape functions into Eqs. (16) and (17), and those can be rewritten as [16,39]

$$\sum_{I=1}^{N_t} \int_{\Gamma_S} \begin{bmatrix} t_{11}^I & t_{12}^I \\ t_{21}^I & t_{22}^I \end{bmatrix} \begin{Bmatrix} x_1^I \\ x_2^I \end{Bmatrix} h_J(Q) d\Gamma = \sum_{I=1}^{N_t} \int_{\Gamma_S} \begin{bmatrix} \Phi_I^t(s) & 0 & \Phi_I^t(s)H(\xi) & 0 \\ 0 & \Phi_I^t(s) & 0 & \Phi_I^t(s)H(\xi) \end{bmatrix} \begin{Bmatrix} t_1^I \\ t_2^I \\ b_1^I \\ b_2^I \end{Bmatrix} h_J(Q) d\Gamma \tag{22}$$

$$\sum_{I=1}^{N_t} \int_{\Gamma_S} \begin{bmatrix} u_{11}^I & u_{12}^I \\ u_{21}^I & u_{22}^I \end{bmatrix} \begin{Bmatrix} x_1^I \\ x_2^I \end{Bmatrix} h_J(Q) d\Gamma = \sum_{I=1}^{N_t} \int_{\Gamma_S} \begin{bmatrix} \Phi_I^u(s) & 0 & \Phi_I^u(s)H(\xi) & 0 \\ 0 & \Phi_I^u(s) & 0 & \Phi_I^u(s)H(\xi) \end{bmatrix} \begin{Bmatrix} u_1^I \\ u_2^I \\ a_1^I \\ a_2^I \end{Bmatrix} h_J(Q) d\Gamma \tag{23}$$

in which $\Phi_I^u(s)$, $\Phi_I^t(s)$ are shape functions for displacement and stress of the present method, and when the calculating node is located on the common calculating boundary, $\Phi_I^u(s) = \Phi_I^t(s)$, when the calculating node is located on crack surface, those two shape functions are constructed by different basis functions, respectively, which can be seen in next section; $H(\xi)$ is the Heaviside enrichment function, which is employed for describing the discontinuity of crack and can be seen in Eq. (42), and $a_1^I$, $b_1^I$ are additional node freedoms for discontinuity.

Using the above equations for all nodes, the system equations can be written in the form

$$\mathbf{Tx} = \mathbf{H}_t\mathbf{t}^{\mathbf{c}} + \mathbf{C}_t\mathbf{b} \tag{24}$$

$$\mathbf{Ux} = \mathbf{H}_u\mathbf{u}^{\mathbf{c}} + \mathbf{C}_u\mathbf{a} \tag{25}$$

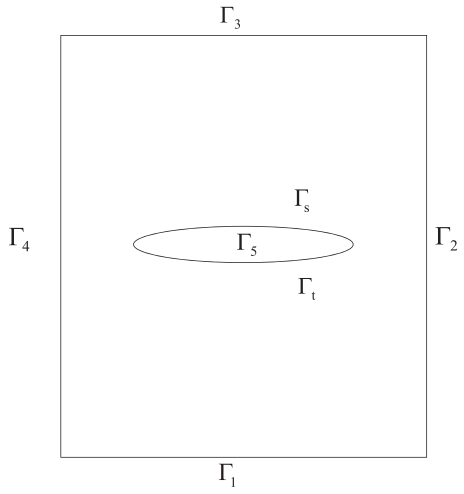


**Fig. 2.** Interpolating segments model.

in which $\mathbf{C}_t = \mathbf{C}_u = \mathbf{0}$ when calculating nodes are located on common boundary, and matrix **T, H, U** can be referred in [16,39], and $\mathbf{t^c}$, $\mathbf{u^c}$ are boundary variable values, and $C_t^{IJ} = \int_{\Gamma_S} \Phi_I^t(s) H(\xi) h_J(Q) d\Gamma$, $C_u^{IJ} = \int_{\Gamma_S} \Phi_I^u(s) H(\xi) h_J(Q) d\Gamma$ when calculating nodes are located on crack surfaces.

## 3. The enriched discontinuous interpolation

In order to overcome the discontinuity of corner and improve the calculation efficiency, the common outer boundary of the model is divided into several segments, which can be seen in Fig. 2, the outer boundary is divided into $\Gamma_1$, $\Gamma_2$, $\Gamma_3$ and $\Gamma_4$, and each segment is interpolated by radial point interpolation method(RPIM).

Firstly, the variable interpolation for continuous boundary is studied, and RPIM is developed to construct shape function for the common continuous boundaries. Unlike the traditional HBNM, the shape function obtained by the present method has the delta function property, so boundary conditions can be applied easily and directly, and computational expense can be greatly reduced. For simplification, the variable $v$ is employed to represent the variables of displacement $u$ and boundary traction $t$, which can be expressed as [37]

$$v(s) \approx v^h(s) = \sum_{i=1}^{N_S} R_i(r) a_i + \sum_{j=1}^{m} P_j(s) b_j = \mathbf{R}^T(\mathbf{r})\mathbf{a} + \mathbf{P}^T(\mathbf{s})\mathbf{b} \tag{26}$$

where $N_S$ is the node number of interpolation segment, $s$ denotes parameter coordinate of boundary curve; and $m$ ($m < N_S$) is the number of monomials basis; $a_i$, $b_j$ are interpolation coefficient; $R_i(r)$ is the RBF, for example: Multi-quadrics (MQ) $R_i(r) = (r_i^2 + c^2)^q$; Gaussian (EXP) $R_i(r) = \exp[-br_i^2]$; Thin plate spline (TPS) $R_i(r) = r_i^n \ln(r_i)$and $P_j(s)$ is the monomial basis $\mathbf{P}^T(\mathbf{s}) = [1, s, s^2]$.

In order to get the constants coefficient $a_i$ and $b_j$, Eq. (35) is enforced to be satisfied at $N_S$ nodes at interpolation segments, which can be expressed as

$$v(s_k) = \sum_{i=1}^{N_S} a_i R_i(r_k) + \sum_{j=1}^{m} b_j P_j(s_k) \quad k = 1, 2, ..., N_S \tag{27}$$

which can be expressed as matrix form

$$v_{\mathbf{0}} = \mathbf{R}_0\mathbf{a} + \mathbf{P}_0\mathbf{b} \tag{28}$$

where the vector of variables is

$$v_0^T = [v(s_1), v(s_2), ..., v(s_{N_S})] \tag{29}$$

The moment matrix of RBFs is [37]

$$\mathbf{R}_0 = \begin{bmatrix} R_1(r_1) & R_2(r_1) & \cdots & R_{N_S}(r_1) \\ R_1(r_2) & R_2(r_2) & \cdots & R_{N_S}(r_2) \\ \vdots & \vdots & \ddots & \vdots \\ R_1(r_{N_S}) & R_2(r_{N_S}) & \cdots & R_{N_S}(r_{N_S}) \end{bmatrix} \tag{30}$$

The monomial moment matrix is

$$\mathbf{P}_0 = \begin{bmatrix} 1 & s_1 & s_1^2 \\ 1 & s_2 & s_2^2 \\ \vdots & \vdots & \vdots \\ 1 & s_{N_S} & s_{N_S}^2 \end{bmatrix} \tag{31}$$

In order to ensure unique solutions, the following constraints are necessary for the present approximation

$$\mathbf{P}_0^T\mathbf{a} = 0 \tag{32}$$

Combining Eqs. (28) and (32) and expressing in matrix form, one can get

$$\tilde{v}_0 = \begin{Bmatrix} v_0 \\ 0 \end{Bmatrix} = \begin{bmatrix} \mathbf{R}_0 & \mathbf{P}_0 \\ \mathbf{P}_0^T & \mathbf{0} \end{bmatrix} \begin{Bmatrix} \mathbf{a} \\ \mathbf{b} \end{Bmatrix} = \mathbf{G}\mathbf{a}_0 \tag{33}$$

where $\mathbf{a}_0^T = [a_1, a_2, ..., a_{N_S}, b_1, b_2 ... b_m]$, $\tilde{v}_0^T = [v(s_1), v(s_2), ..., v(s_{N_S}), 0, 0, 0]$, $\mathbf{G} = \begin{bmatrix} \mathbf{R}_0 & \mathbf{P}_0 \\ \mathbf{P}_0^T & \mathbf{0} \end{bmatrix}$.

Then we can get [37]

$$v(s) = [\mathbf{R}^T(\mathbf{r}) \quad \mathbf{P}^T(\mathbf{s})]\mathbf{G}^{-1}\tilde{v}_0 = \tilde{\mathbf{\Phi}}(\mathbf{s})\tilde{v}_0 \tag{34}$$

in which $\tilde{\mathbf{\Phi}}^T(\mathbf{s}) = [\mathbf{R}^T(\mathbf{r}) \quad \mathbf{P}^T(\mathbf{s})]\mathbf{G}^{-1} = [\Phi_1(s), \Phi_2(s), ..., \Phi_{N_S}(s), ..., \Phi_{N_S+m}(s)]$.

Finally, the shape function of the present method, which is obtained by RPIM, is given as

$$\mathbf{\Phi}^T(\mathbf{s}) = [\Phi_1(s), \Phi_2(s), ..., \Phi_{N_S}(s)] \tag{35}$$

So the displacement and normal traction of boundary nodes on the common continuous boundary can be obtained as

$$\tilde{u}(s) = \mathbf{\Phi}^T(\mathbf{s})\mathbf{u} = \sum_{i=1}^{N_S} \Phi_i(s) u_i \tag{36}$$

$$\tilde{t}(s) = \mathbf{\Phi}^T(\mathbf{s})\mathbf{t} = \sum_{i=1}^{N_S} \Phi_i(s) t_i \tag{37}$$

In which $\mathbf{u}^T = [u_1, u_2, ..., u_{N_S}]$, $\mathbf{t}^T = [t_1, t_2, ..., t_{N_S}]$ are nodes values of boundary nodes.

For discontinuous crack segment $\Gamma_5$, crack $\Gamma_5$ is consist with the upper crack surface $\Gamma_s$ and the bottom crack surface $\Gamma_t$, an enriched discontinuous interpolation is developed in this method. As we know, displacement field and stress field around crack tip are singular or nonlinear. Using the traditional RPIM, we can hardly get the accurate results. In order to accurately simulate the high gradient displacements near crack tip, we use the enriched basis functions combining with RPIM when the approximating nodes are near enough to crack tip, and the fully enriched basis functions for boundary displacement variable are given as [27]

$$\mathbf{p^T}(\mathbf{s}) = \left[1, s, s^2, \sqrt{r}\cos\frac{\theta}{2}, \sqrt{r}\sin\frac{\theta}{2}, \sqrt{r}\sin\frac{\theta}{2}\sin\theta, \sqrt{r}\cos\frac{\theta}{2}\sin\theta\right] \tag{38}$$

For simplification, the radial basis function can be given as

$$\mathbf{p^T}(\mathbf{s}) = [1, s, s^2, \sqrt{r}] \tag{39}$$

In this method, hybrid basis function is used, when nodes are located nearby crack tip, the enriched basis function is used to approximate the variables, and for nodes far away from crack tip the quadratic basis function is used. Substituting Eq. (39) into Eq. (28), one can get the traditional continuous part of shape function for boundary displacement, which is

$$\tilde{u}_{\Gamma_5}(s) = \sum_{i=1}^{N_S} \Phi_i^u(s) u_i \tag{40}$$

In which $\Phi_i^u(s)$ is the continuous part of shape function related to Eq. (39).

As we know, displacement and stress on segment $\Gamma_5$ are discontinuous. Based on partition of unity, the shape function of boundary displacement for discontinuous boundary can be given as

$$\tilde{u}(s) = \sum_{i=1}^{N_S} \Phi_i^u(s) u_i + \sum_{j=1}^{N_S} \Phi_j^u(s) H(\xi) \mathrm{a}_j \tag{41}$$

In which $a_j$ is the additional degree of nodal freedom for modeling strong discontinuity.

It is known to us that the displacements on the nodes of the upper and bottom surfaces of crack are different, in order to model the strong discontinuity caused by crack, the signed function is chosen as the Heaviside enrichment function, which is given as

$$H(\xi) = \begin{cases} 1 & \forall \xi \in \Gamma_s \\ -1 & \forall \xi \in \Gamma_t \end{cases} \tag{42}$$

In which $\xi$ is the location function of calculation node.

As we know, the boundary displacement and traction in the present method are interpolated, respectively, so for high gradient stress near crack tip for mixed mode crack can be given as [7]

$$\sigma_{xx} = \frac{K_I}{\sqrt{2\pi r}} \cos\frac{\theta}{2}\left(1 - \sin\frac{\theta}{2}\sin\frac{3\theta}{2}\right) + \frac{K_{II}}{\sqrt{2\pi r}} \sin\frac{\theta}{2}\left(2 + \cos\frac{\theta}{2}\cos\frac{3\theta}{2}\right) \tag{43}$$

$$\sigma_{yy} = \frac{K_I}{\sqrt{2\pi r}} \cos\frac{\theta}{2}\left(1 + \sin\frac{\theta}{2}\sin\frac{3\theta}{2}\right) + \frac{K_{II}}{\sqrt{2\pi r}} \sin\frac{\theta}{2}\cos\frac{\theta}{2}\cos\frac{3\theta}{2} \tag{44}$$

Based on Eqs. (43) and (44), the fully enriched basis function for boundary traction variable can be given as

$$\mathbf{p^T(s)} = \left[1, s, s^2, \cos\frac{\theta}{2}/\sqrt{r}, \sin\frac{\theta}{2}/\sqrt{r}, \sin\frac{3\theta}{2}\sin\theta/\sqrt{r}, \sqrt{r}\cos\frac{3\theta}{2}\sin\theta/\sqrt{r}\right] \tag{45}$$

Substituting Eq. (45) into Eq. (28), one can get the traditional continuous part of shape function for boundary traction, which is

$$\tilde{t}_{\Gamma_5}(s) = \sum_{i=1}^{N_S} \Phi_i^t(s) t_i \tag{46}$$

In which $\Phi_i^t(s)$ is the continuous part of shape function related to Eq. (45).

As we know, the displacement and stress on segment $\Gamma_5$ is discontinuous. Based on partition of unity, the shape function of boundary traction for discontinuous boundary can be given as

$$\tilde{t}(s) = \sum_{i=1}^{N_S} \Phi_i^t(s) t_i + \sum_{j=1}^{N_S} \Phi_j^t(s) H(\xi) \mathrm{b}_j \tag{47}$$

In which $b_j$ is the additional degree of nodal freedom for modeling strong discontinuity of boundary tractions.

## 4. Numerical implementation

In the above section, the complementary solution has been solved successfully. Now the particular solution will be developed by dual reciprocity method. Actually, the particular solution is the solution of Eq. (8).

### 4.1. Dual reciprocity method

DRM can be used in elasticity to transform the domain integral arising from the application of body force into equivalent boundary integrals. According to the interpolation, the approximation of the term $b_k(k=1,2)$ can be proposed as [37]

$$b_k \approx \sum_{j=1}^{N+L} f^j \alpha_k^j \tag{48}$$

where, $\alpha_k^j$ are a set of unknown coefficients, $f^j$ are the approximation functions, $N$ and $L$ are the total numbers of boundary nodes and interior nodes, respectively.

Eq. (48) can be rewritten as

$$\boldsymbol{\alpha} = \mathbf{F^{-1}b} \tag{49}$$

where vector $\mathbf{b}$ is the values of body force term on each calculation nodes, and matrix $\mathbf{F}$ is the values of approximating function on each nodes pairs.

Also, the particular solutions of the displacement can be interpolated by the particular solution of basis form [37]

$$u_k^p \approx \sum_{j=1}^{N+L} \alpha_l^j \bar{u}_{lk}^j \tag{50}$$

where $\bar{u}_{lk}^j$ is the basis form of particular solution.

If $u_k^p$ satisfies Eq. (8), the following equation can be obtained

$$G\bar{u}_{mk,ll}^j + \frac{G}{1-2\nu}\bar{u}_{lk,lm}^j = \delta_{mk} f^j \tag{51}$$

The approximating function, $f$, can be chosen as, $f^j = 1 + r$. So the basis form of particular solution $\bar{u}_{km}$ satisfying Eq. (51) is given by [37]

$$\bar{u}_{km} = \frac{1-2\nu}{(5-4\nu)G} r_{,m} r_{,k} r^2 + \frac{1}{30(1-\nu)G}\left[\left(3 - \frac{10\nu}{3}\right)\delta_{mk} - r_{,m} r_{,k}\right] r^3 \tag{52}$$

The corresponding expression for the traction $\bar{t}_{km}$ is

$$\begin{aligned} \bar{t}_{km} = {} & \frac{2(1-2\nu)}{(5-4\nu)}\left[\frac{1+\nu}{1-2\nu} r_{,m} n_k + \frac{1}{2} r_{,k} n_m + \frac{1}{2}\delta_{mk}\frac{\partial r}{\partial n}\right] r \\ & + \frac{1}{15(1-\nu)}\left[(4-5\nu) r_{,k} n_m - (1-5\nu) r_{,m} n_k \right. \\ & \left. + \left[(4-5\nu)\delta_{mk} - r_{,m} r_{,k}\right]\frac{\partial r}{\partial n}\right] r^2 \end{aligned} \tag{53}$$

Solving Eqs. (49) and (50), the particular solutions can be written as

$$u_i^p = \sum_{I=1}^{N+L} \begin{bmatrix} \bar{u}_{11}^I & \bar{u}_{12}^I \\ \bar{u}_{21}^I & \bar{u}_{22}^I \end{bmatrix} \begin{Bmatrix} \alpha_1^I \\ \alpha_2^I \end{Bmatrix} \tag{54}$$

$$t_i^p = \sum_{I=1}^{N+L} \begin{bmatrix} \bar{t}_{11}^I & \bar{t}_{12}^I \\ \bar{t}_{21}^I & \bar{t}_{22}^I \end{bmatrix} \begin{Bmatrix} \alpha_1^I \\ \alpha_2^I \end{Bmatrix} \tag{55}$$

Substituting Eq. (49) into Eqs. (54) and (55), one can obtain the particular solution in matrix form as

$$\mathbf{u^p} = \mathbf{VF^{-1}b} \tag{56}$$

$$\mathbf{t^p} = \mathbf{QF^{-1}b} \tag{57}$$

where $\mathbf{V}$ and $\mathbf{Q}$ are the matrices of the basic form of particular solution.

Substituting Eqs. (56) and (57) into Eqs. (10) and (11), one can obtain the complementary solution in matrix form

$$\mathbf{u^c} = \mathbf{u} - \mathbf{u^p} = \mathbf{u} - \mathbf{VF^{-1}b} \tag{58}$$

$$\mathbf{t^c} = \mathbf{t} - \mathbf{t^p} = \mathbf{t} - \mathbf{QF^{-1}b} \tag{59}$$

Appling dual reciprocity method, the domain integral of body force term can be transferred into the boundary integral. Using Eqs. (58) and (59) for the common calculating boundary, Eqs. (24) and (25) become

$$\mathbf{Tx} = \mathbf{H}\left(\mathbf{t} - \mathbf{t^p}\right) \tag{60}$$

$$\mathbf{Ux} = \mathbf{H}\left(\mathbf{u} - \mathbf{u^p}\right) \tag{61}$$

In this paper, we assume that the crack is always opening, then on crack surface, we get the following relation

$$t_n = t_t = 0 \qquad on \quad \Gamma_s \quad , \Gamma_t \tag{62}$$

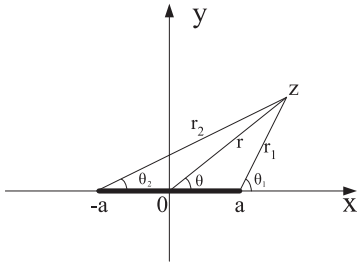


**Fig. 3.** Local coordinate system of crack tip.

in which the subscript *n, t* represent the normal direction and tangential direction, respectively. On boundary $\Gamma_5$, we can get

$$\mathbf{Tx} = \mathbf{H}_t\left(\mathbf{t} - \mathbf{t}^{\mathbf{p}}\right) + \mathbf{C}_t\mathbf{b} \tag{63}$$

$$\mathbf{Ux} = \mathbf{H}_u\left(\mathbf{u} - \mathbf{u}^{\mathbf{p}}\right) + \mathbf{C}_u\mathbf{a} \tag{64}$$

in which $\mathbf{H}_t$, $\mathbf{H}_u$ are matrix related to shape function of Eqs. (47) and (41), respectively.

Based on the additional boundary condition of Eq. (62) and system equations of Eqs. (63) and (64), we get some additional equations, then additional freedom $a_j$ and $b_j$ can be solved.

### 4.2. Stress intensity factor solving

There are many methods for calculating stress intensity factor for crack problems, and the simplest one is two point displacement formulation, and one of the most accurate one is the J-integral. In this paper, the directly displacement extrapolation around crack tip is used to calculate stress intensity factors $K_I$ and $K_{II}$. According to elastic fracture mechanics, the displacement field around crack tip is given as [7]

$$u_x = \frac{K_I}{4\mu}\sqrt{\frac{r_1}{2\pi}}\left[(2\kappa-1)\cos\frac{\theta_1}{2} - \cos\frac{3\theta_1}{2}\right] + \frac{K_{II}}{4\mu}\sqrt{\frac{r_1}{2\pi}}\left[(2\kappa+3)\sin\frac{\theta_1}{2} + \sin\frac{3\theta_1}{2}\right] \tag{65}$$

$$u_y = \frac{K_I}{4\mu}\sqrt{\frac{r_1}{2\pi}}\left[(2\kappa+1)\sin\frac{\theta_1}{2} - \sin\frac{3\theta_1}{2}\right] - \frac{K_{II}}{4\mu}\sqrt{\frac{r_1}{2\pi}}\left[(2\kappa-3)\cos\frac{\theta_1}{2} + \cos\frac{3\theta_1}{2}\right] \tag{66}$$

In which $\kappa = 3-4\nu$ for plane strain problems and $\kappa = 3-4\nu$ for plane stress problems, and and $\theta_1$ is the local coordinate around crack tip, which is shown in Fig. 3.

Via DHBNM, the displacement of crack tip nodes can be got. According to the numerical results $u_x(r_1,\pi)$ and $u_y(r_1,\pi)$, in which $r_1$ satisfies

$$0.008 \le \frac{r_1}{a} \le 0.013 \tag{67}$$

Using extrapolation method, we can get the stress intensity factors via Eq. (67) when $r_1 \to 0$.

## 5. Numerical examples

A number of examples are presented to illustrate the effectiveness of this method for linear elastic crack problems analysis. The results of the present method are compared with both the analytical solutions and those obtained by some other methods and some published results.

In these examples, the support size for the weight function $d_I$ is taken to be $3.5h$, the radius of the sub-domain $r_J$ is chosen as $0.85h$, with $h$ being the average distance of the adjacent nodes. The parameter $c_I$ is taken to be $d_I/c_I = 0.5$, and the parameter $c_J$ is taken to be $r_J/c_J = 1.2$, and the influence of those parameters can be seen in the previous work of author ([36,38], 2010, [33]).

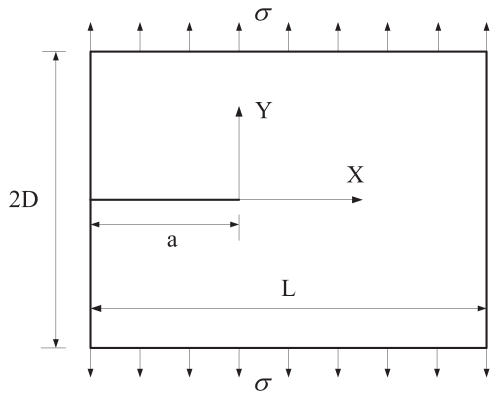


**Fig. 4.** A unidirectional plate with a crack under uniform loading.

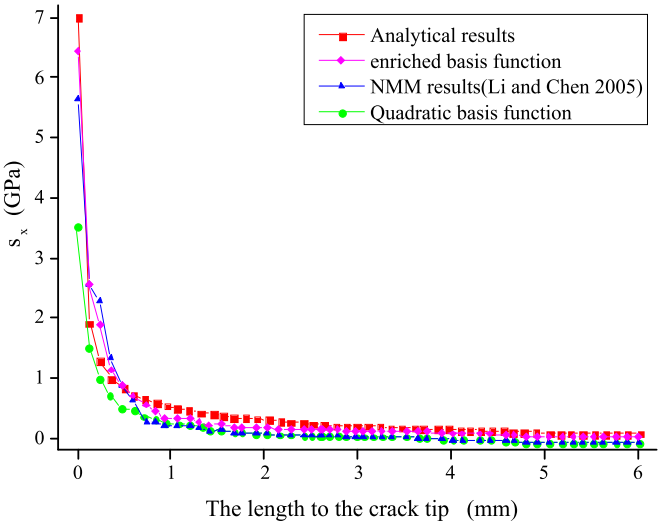


**Fig. 5.** $\sigma_x$ at the tip of the crack.

### 5.1. An edge-cracked plate under pure tension

Consider an edge-cracked plate under pure tension as shown in Fig. 4 [10], which has the length, $2D = 20$ mm, width, $L = 52$ mm, and crack length $a = 12$ mm. The far field tensile stress, $\sigma = 0.2$ GPa. The plane stress problem is considered, and the material property are given as: $E = 76$ GPa, $\mu = 0.286$. Due to symmetry, only half of the plate was analyzed. In the present calculation, 100 boundary nodes are used, and the results obtained by different basis functions are used for comparison.

For convenience, the regulated stress intensity factor is used, which is given as $\tilde{K}_I = K_I/(\sigma\sqrt{a\pi})$. For the same number of boundary nodes, the regulated stress intensity factors which obtained by different basis function is given as Table 1, in which the results obtained by reference [10] are used for comparison and the analytical result is 1.44. It is shown that the results obtained by fully enriched basis function and hybrid enriched basis function are much more close to the analytical results and published results.

The $\sigma_x$, $\sigma_y$ near crack tip by different basis function are given in Figs. 5 and 6, in which the analytical results and those obtained by numerical manifold method (NMM) [10] are given for comparison. It is shown in those figures that a good agreement is achieved between those results, especial for the results that enriched basis function is used.

### 5.2. A central inclined cracked plate under tension

It is shown in Fig. 7, a angle-cracked plate with the length $2b = 20$ m and the width $2h = 30$ m. There is an inclined crack in the center of the

**Table 1**
Mode –I stress intensity factor using different basis functions.

| Type of basis function | The present method $\tilde{K}_I$ | Relative error (%) | NMM [10] $\tilde{K}_I$ | Relative error (%) |
|---|---|---|---|---|
| Quadratic | 1.37 | 4.9 | 1.32 | 8.2 |
| Fully enriched | 1.428 | 0.83 | 1.41 | 1.5 |
| Radial enriched | 1.416 | 1.66 | 1.41 | 1.5 |
| Hybrid enriched | 1.430 | 0.69 | 1.41 | 1.5 |

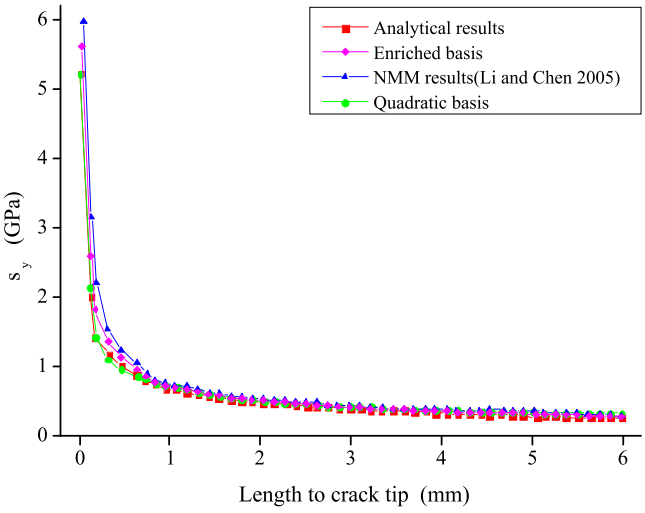


**Fig. 6.** $\sigma_y$ at the tip of the crack.

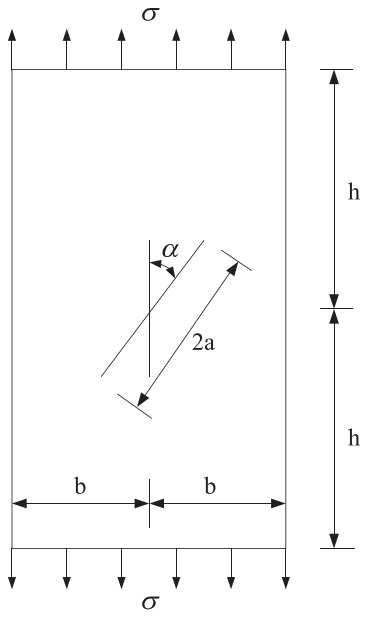


**Fig. 7.** A central inclined cracked plate under tensile.

plate with the length is $2a=3$ m, and the angle between crack direction and vertical direction is $\alpha$. The far field tensile is $\sigma=1$ Pa. The analytical solutions are [6]

$$K_I = \sigma\sqrt{\pi a}\sin^2\alpha \tag{68}$$

$$K_{II} = \sigma\sqrt{\pi a}\sin\alpha\cos\alpha \tag{69}$$

The same as example 5.1, 60 boundary nodes are arranged on the boundary and 30 nodes on the crack. The results on different inclined angles are given in Table 2, in which $\tilde{K}_I = K_I/K_I^A$, where $K_I^A$ is the

**Table 2**
Stress intensity factors of central inclined plate under tensile.

| Angle $\alpha$ | $\tilde{K}_I$ | | $\tilde{K}_{II}$ | |
|---|---|---|---|---|
| | The present method | XFEM [6] | The present method | XFEM [6] |
| 15 | 1.021 | 1.034 | 1.013 | 0.979 |
| 30 | 1.009 | 1.011 | 1.005 | 1.006 |
| 45 | 1.007 | 0.991 | 1.028 | 0.922 |
| 60 | 1.011 | 1.017 | 1.007 | 1.013 |
| 75 | 1.014 | 1.019 | 1.020 | 1.033 |

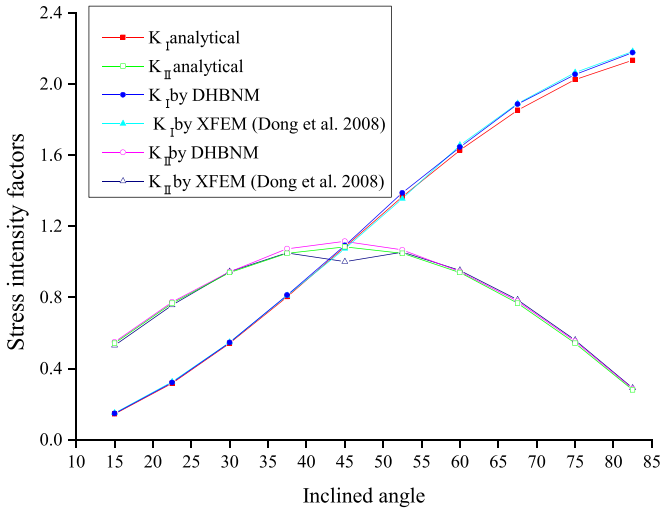


**Fig. 8.** Stress intensity factors of central inclined plate on different angles.

analytical results which given as Eq. (68). For comparison, the results which are obtained by extended finite element method [6] are also given in Table 2. It is shown that a great agreement can be achieve between the present method, those of extended finite element method (XFEM) and analytical results.

The stress intensity factors obtained by different inclined angles by the present method, those of analytical results and those obtained by XFEM [6] are shown in Fig 8, in which we can see that the results obtained by those methods are close to each other.

### 5.3. Panel with doubly cracked hole

In order to further illustrate the effectiveness of this method, we examine the uniaxial stressing of a panel which contains a doubly-cracked hole as shown in Fig. 9, which is subjected to an uniaxial tension $\sigma$. The geometry of this problem satisfies the following equations, $2h/w=a/r=1$, $2(r+a)=\frac{1}{2}w$. Chang and Mear [5] and Pan [22] solved this problem by forming a single-domain BEM.

For this problem, we use 60 outer boundary nodes, 30 nodes on hole boundary and 30 nodes on crack. The solutions obtained by the present method and those determined by Chang and Mear [5] and Pan [22] are given in Table 3, which again shows excellent agreement between those three methods.

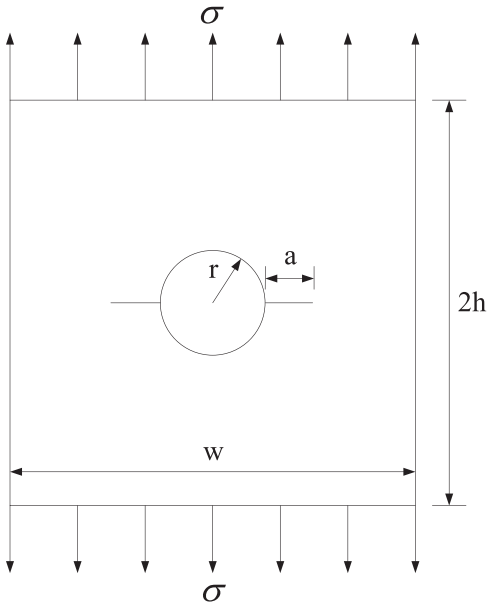


**Fig. 9.** Double edge cracks emanating from a hole in a rectangular.

**Table 3**
SIF $K_I/\sigma\sqrt{\pi(r+a)}$ of double edge cracks.

| Method | $K_I/\sigma\sqrt{\pi(r+a)}$ |
|---|---|
| DHBNM with Quadratic basis | 1.6029 |
| DHBNM with enriched basis | 1.5632 |
| Chang and Mear [5] | 1.5627 |
| Pan [22] | 1.5636 |

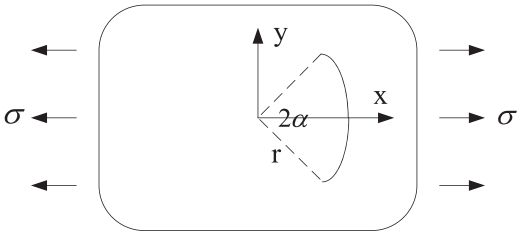


**Fig. 10.** Model of circular-arc crack plate.

### 5.4. Arc crack

Consider a circular-arc crack of radius r embedded in an infinite domain, which is shown in Fig. 10. The center of the circular arc is the origin of the coordinate system, and the midpoint of the crack is located on the x-axis, and the angle of the arc is $2\alpha$. For this model, a uniaxial tensile is applied in the x-direction. At this time, the mode one and mode two stress intensity factors are functions of $\alpha$.

In the present calculation, 60 nodes are used on arc crack. The results for different angles of the present method and exact solutions [17] are shown in Fig. 11, in which $F = \frac{K}{\sigma\sqrt{\pi r \sin\alpha}}$. It is shown that the results obtained by those two methods are close to each other.

In Table 4, the stress intensity factors are compared with exact values for particular angle $\alpha = 45^{\circ}$. It can be see that an excellent agreement is achieved between those methods.

## 6. Conclusions

A new boundary node meshless method named as discontinuous dual hybrid boundary node method is proposed. It combines the hybrid boundary node method, dual reciprocity method and discontinuous shape function constructing method. HBNM is used to solve the complementary solution of homogeneous equation, and DRM is used to deal with the inhomogeneous terms. The boundary integral equation is discretized using the meshless shape functions based on a group of arbitrarily distributed points on the boundary. It does not require any element connectivity for constructing the shape function, and thus possesses the dimensionality reduction advantage. The present work uses directly displacement extrapolation to calculate stress intensity factors. Besides, the boundary is divided into several individual segments, and each one of those segments is interpolated, respectively. For continuous segments, radial point interpolation method is employed. In regard to discontinuous segments, the enriched discontinuous basis functions in radial point interpolation method are presented for simulating discontinuity of displacement and stress field on surfaces of fracture, and the near tip asymptotic field function is employed for simulating the singularity of the crack tip stress field around the crack tip. So that high accuracy and discontinuity property of the crack can be easily described in the present method.

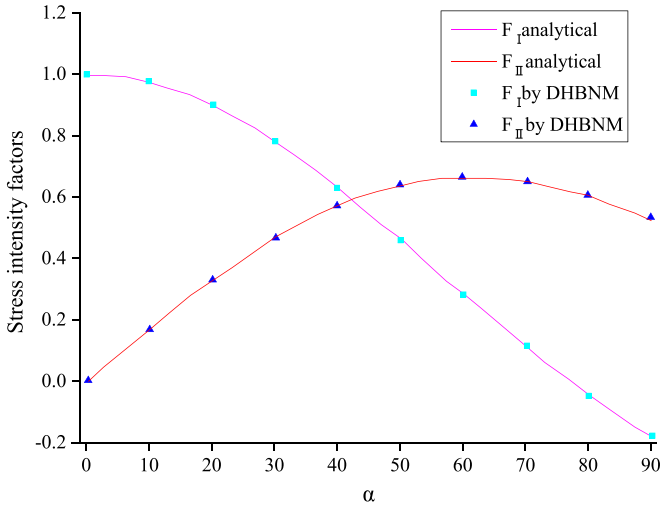


**Fig. 11.** Normalized stress intensity factors for arc crack on different angles.

**Table 4**
Normalized stress intensity factors for arc crack on $\alpha = 45^{\circ}$.

| Crack element or nodes | The present method | | BEM [17] | |
|---|---|---|---|---|
| | $K_I/K_I^{exa}$ | $K_{II}/K_{II}^{exa}$ | $K_I/K_I^{exa}$ | $K_{II}/K_{II}^{exa}$ |
| 20 | 1.028 | 1.012 | 1.045 | 1.011 |
| 40 | 1.016 | 1.009 | 1.017 | 1.012 |
| 50 | 1.009 | 1.007 | 1.010 | 1.009 |
| 60 | 1.007 | 1.008 | 1.007 | 1.007 |

Both single mode and mixed mode problems can be solved by this method. A number of examples are presented to evaluate the accuracy of the stress intensity factors calculated by this method, and comparisons are made between the results obtained by this method and some published results. The numerical examples are shown that the present method is effective and can be widely applied in practical engineering.

The main advantage of the present method compared to the traditional DHBNM is that a discontinuous structure can be considered and no extra remeshing and integral technique are needed, then the present method can be easily used for crack propagation, contact problem and excavation for rock engineering, and the present method will be employed in crack propagation for rock and concrete engineering, excavation and interface problems for rock engineering and crack contact, cohesive problem in practical engineering.

## Acknowledgment

The work was financially supported by the National Natural Science Foundation of China (Nos. 11232014 and 51621006), the State Key Research Development Program of China (No. 2016YFC0600707), the International Partnership Program of Chinese Academy of Sciences (115242KYSB20160017), and Youth Innovation Promotion Association CAS (No. 2014304).

## References

[1] Armero F, Linder C. Numerical simulation of dynamics fracture using finite elements with embedded dicontinuities. Int J Fract 2009;160:119–41.
[2] Atluri SN, Sladek J, Sladek V, Zhu T. The local boundary integral equation and it's meshless implementation for linear elasticity. Comput Mech 2000;25:180–98.
[3] Atluri SN, Zhu T. A new meshless local Petrow-Galerkin approach in computational mechanics. Comput Mech 1998;22:117–27.
[4] Belytschko T, Lu YY, Gu L. Element-free Galerkin methods. Int J Numer Methods Eng 1994;37:229–56.
[5] Chang CC, Mear ME. A boundary element method for two dimensional linear elastic fracture analysis. Int J Fract 1995;74:219–51.
[6] Dong YW, Yu TT, Ren QW. Extended finite element method for direct evaluation of strength intensity factors. Chin J Comput Mech 2008;25(1):72–7.
[7] Fedelinski P, Aliabadi MH. The dual boundary element method: $\hat{J}$ integral for dynamic stress intensity factors. Int J Fract 1994;65:369–81.
[8] Gu Y, Chen W, Gao H, Zhang C. A meshless singular boundary method for three-dimensional elasticity problems. Int J Numer Methods Eng 2016;107:109–26.
[9] Gu Y, Chen W, He XQ. Improved singular boundary method for elasticity problems. Comput Struct 2014;135:73–82.
[10] Li SC, Chen YM. Numerical manifold method for crack tip fields. Chin Civil Eng J 2005;38(7):96–102.
[11] Libersky LD, Petschek AG, Camey TC, et al. High strain Lagrangian hydrodynamics. J Comput Phys 1993;109:67–75.
[12] Lu YY, Belytschko T, Gu L. A new implementation of the element free Galerkin method. Comput Methods Appl Mech Eng 1994;113:397–414.
[13] Miao Y, Wang YH, Yu F. Development of hybrid boundary node method in two-dimensional elasticity. Eng Anal Bound Elements 2005;29:703–12.
[14] Moes N, Dolbow J, Belytschko T. A finite element method for crack growth without remeshing. Int J Numer Methods Eng 1999;46:131–50.
[15] Monaghan JJ. An introduction to SPH. Comput Phys Commun 1988;48:89–96.
[16] Mukherjee YX, Mukherjee S. The boundary node method for potential problems. Int J Numer Methods Eng 1994;140:797–815.
[17] Muskhelishvili NI. Some basic problems of the mathematical theory of elasticity. Groningen: Noordhoff; 1963.
[18] Nardini D, Brebbia CA. Boundary integral formulation of mass matrices for dynamic analysis. Topics in boundary element research, Vol. 2. Berlin and New Yorks: Springer-Verlag; 1985.
[19] Nayroles B, Touzot G, Villon P. Generalizing the finite element method: diffuse approximation and diffuse elements. Comput Mech 1992;10:307–18.
[20] Oliver J. Modeling strong discontinuities in solid mechanics via strain softening constitutive equations, part I: fundamentals. Int J Numer Methods Eng 1996;39:3575–600.
[21] Oliver J, Huespe AE, Pulido MDG, Chaves E. From continuum mechanics to fracture mechanics: the strong discontinuity approach. Eng Fract Mech 2002;69:113–36.
[22] Pan E. A general boundary element analysis of 2-D linear elastic fracture mechanics. Int J Fract 1997;88:41–59.
[23] Pan E, Amadei B. Fracture mechanics analysis of cracked 2-D anisotropic media with a new formulation of the boundary element method. Int J Fract 1996;77:161–74.
[24] Portela A, Aliabadi MH, Rooke DP. The dual boundary element method: effective implementation for crack problems. Int J Numer Methods Eng 1992;33(6):1269–87.
[25] Prasad NNV, Aliabadi MH, Rooke DP. The dual boundary element method for thermoelastic crack problems. Int J Fract 1994;66:255–72.
[26] Racz D, Bui QT. Novel adaptive meshfree integration techniques in meshless methods. Int J Numer Methods Eng 2012;90:1414–34.
[27] Rao BN, Rahman S. An efficient meshless method for fracture analysis of cracks. Comput Mech 2000;26:398–408.
[28] Simone A, Wells G, Sluys L. From continuous to discontinuous failure in a gradient-enhanced continuum damage model. Comput Methods Appl Mech Eng 2003;192:4581–607.
[29] Stolarska M, Chopp DL, Moes N, Belytschko T. Modelling crack growth by level sets in the extended finite element method. Int J Numer Methods Eng 2001;51:943–60.
[30] Wang HT, Yao ZH, Cen S. A meshless singular hybrid boundary node method for 2-D elastostatics. J Chin Inst Eng 2004;27:481–90.
[31] Wrobel LC, Brebbia CA. The dual reciprocity boundary element formulation for non–linear diffusion problems. Comput Methods Appl Mech Eng 1987;65(2):147–64.
[32] Yan F, Feng XT, Lv JH, Pan PZ. A new hybrid boundary node method based on Taylor expansion and Shepard interpolation method. Int J Numer Methods Eng 2015;102:1488–506.
[33] Yan F, Feng XT, Zhou H. Dual reciprocity hybrid radial boundary node method for the analysis of Kirchhoff plates. Appl Math Model 2011;35(12):5691–706.
[34] Yan F, Feng XT, Zhou H. A dual reciprocity hybrid radial boundary node method based on radial point interpolation method. Comput Mech 2010;45:541–52.
[35] Yan F, Feng XT, Zhou H. Meshless method of dual reciprocity hybrid radial boundary node method for elasticity. Acta Mech Solida Sin 2010;23:447–58.
[36] Yan F, Wang YH, Miao Y, Tan F. Dual reciprocity hybrid boundary node method for three-dimensional elasticity with body force. Acta Mech Solida Sin 2008;21(3):267–77.
[37] Yan F, Wang YH, Miao Y, Tham LG, Cheung YK. Dual reciprocity hybrid boundary node method for free vibration analysis. J Sound Vib 2009;321(3-5):1036–57.
[38] Yan F, Wang YH, Tham LG, Cheung YK. Dual reciprocity hybrid boundary node method for 2-D elasticity with body force. Eng Anal Bound Elements 2008;32(9):713–25.
[39] Zhang JM, Yao ZH, Li H. A hybrid boundary node method. Int J Numer Methods Eng 2002;53:751–63.
[40] Zhang JM, Yao ZH, Masataka T. The meshless regular hybrid boundary node method for 2-D linear elasticity. Eng Anal Bound Elements 2003;127:259–68.
[41] Zhang JM, Yao ZH. The regular hybrid boundary node method for three-dimensional linear elasticity. Eng Anal Bound Elements 2004;28:525–34.
[42] Zhang JM, Yao ZH. Meshless regular hybrid boundary node method. Comput Model Eng Sci 2001;2:307–18.